Giant resonance in transitional nuclei: Photoneutron cross sections for osmium isotopes

B. L. Berman, D. D. Faul, R. A. Alvarez, P. Meyer, and D. L. Olson
Lawrence Livermore Laboratory, University of California, Livermore, California 94550
(Received 7 August 1978)

Photoneutron cross sections, including $\sigma[(\gamma,n) + (\gamma,pn)]$, $\sigma[(\gamma,2n) + (\gamma,p2n)]$, and $\sigma(\gamma,3n)$, were measured for ^{188}Os, ^{189}Os, ^{190}Os, and ^{192}Os from 7 to 30 MeV and for ^{186}Os from 11 to 20 MeV, with a photon energy resolution of about 300 keV. The source of radiation was the monoenergetic photon beam obtained from the annihilation in flight of fast positrons. The partial photoneutron cross sections were determined by neutron multiplicity counting, and the average neutron energies for each multiplicity were determined simultaneously with the cross-section data by the ring-ratio technique. Nuclear information extracted from the data includes parameters of the giant dipole and giant quadrupole resonances, integrated cross sections and their moments, nuclear symmetry energies, and nuclear deformation parameters and intrinsic quadrupole moments. No fewer than eight kinds of evidence point to a sudden change of behavior between ^{189}Os and ^{190}Os, which could be interpreted as a phase transition from a statically deformed prolate nucleus to a γ-unstable one, in general (but not detailed) agreement with the prediction of a dynamic-collective-model calculation.

[NUCLEAR REACTIONS ^{186,188,189,190,192}Os$(\gamma,n,2n,3n)$, E_γ=7–30 MeV; measured 4π neutron yield, multiplicities, average energies for monenergetic photons; $\sigma(E_\gamma,1n)$, $\sigma(E_\gamma,2n)$, $\sigma(E_\gamma,3n)$, GDR parameters, nuclear shape parameters, integrated cross sections and moments, GQR parameters, nuclear phase transition.]

I. INTRODUCTION

The study of the giant dipole resonance (GDR) for nuclei in the transitional region near $A = 190$ can provide a sensitive measure of the behavior of the nuclear shape there. In particular, such a study, particularly for the osmium ($Z = 76$) isotopes, might indicate, through an examination of the evolution of the GDR as one adds neutrons to the lightest osmium nuclei, which presumably are statically deformed and prolate, whether and where a phase transition takes place, how sharply it takes place, and what the nature of such a phase transition might be. In particular, theoretical work has speculated that the heavier osmium isotopes are triaxial, oblate, or γ-unstable (which can be thought of as prolate part of the time and oblate the rest of the time). The GDR for a statically deformed triaxial nucleus (see, for example, Ref. 1) would contain three peaks, corresponding to dipole vibrations along each of the three nuclear axes, in much the same way as the GDR for a spheroidal nucleus has two.[2-4] The GDR for an oblate nucleus would be characterized by the fact that the area of the lower-energy peak, which corresponds to dipole vibrations along either of the long axes of the nucleus, would be twice as large as that of the higher-energy peak, which corresponds to vibrations along the short axis. This behavior is opposite to that for prolate nuclei, where this area ratio R_A is one-half instead of two, and for which the intrinsic quadrupole moment Q_0 is positive instead of negative, as it is for oblate nuclei. [It should be noted here that the decomposition of the GDR for a deformed nucleus into two peaks thus gives the *sign* of Q_0 (in addition to its magnitude[3]), unlike Coulomb-excitation measurements, which yield only the value for Q_0^2. Moreover, values for Q_0 for odd-A nuclei also can be determined by this method.] Kumar and Baranger[5] have employed the pairing-plus-quadrupole model to construct potential energy surfaces and from them to calculate a number of properties of nuclei across the entire region of deformed nuclei (with $N = 82$ to 126 and $Z = 50$ to 82), including values for Q_0. In particular, they predict that for the osmium isotopes there is a gradual transition from prolate to oblate shapes: ^{186}Os ($N = 110$) is predicted to be prolate, ^{188}Os and ^{190}Os asymmetric ($\gamma \neq 0$), and ^{192}Os ($N = 116$) oblate. These shapes result in predictions for Q_0 that change sign sharply between ^{188}Os and ^{190}Os, from about +4.5 to −4.5 b, respectively. This sharp transition for Q_0 should be reflected in the values for R_A for these nuclei. The GDR for a γ-unstable nucleus, for which the ground-state wave function has roughly equal prolate and oblate components, would be characterized by a shape related intimately to its spectrum of low-energy excited states, and would be composed of a family of overlapping peaks combining the features of the prolate and oblate cases. Sedlmayr *et al.*[6] have

performed a detailed calculation, for all the even-A osmium isotopes, of the shape of the GDR. They did this by constructing the potential-energy surface for each of these nuclei by fitting a part of its low-energy spectrum and then using these potential-energy surfaces to deduce the collective Hamiltonian for each nucleus, from which they were able to compute, using the dynamic collective model, among other things, the energies and strengths (but not the widths) for the dipole absorption lines for each nucleus. By assigning an arbitrary width (of 1.5 MeV) to each line, Sedlmayr *et al.* produced predictions for the shapes of the GDR for the even osmium isotopes, which can be compared with the experimental results.

There is also the question of the existence, location, and behavior (such as splitting) of the isovector ($\Delta T = 1$) giant quadrupole resonance (GQR) for transitional nuclei such as the osmium isotopes. Theoretical calculations[7-9] which have been compared with previous experimental results from this laboratory[10-12] have achieved extraordinarily good fits to the data, and therefore the isovector GQR merits serious consideration as the explanation for structure seen at energies above the GDR for a number of medium and heavy nuclei. It is therefore interesting to see if such high-energy structure exists for the transitional osmium isotopes, and if so to delineate its evolution as well as that of the GDR itself.

Previous experimental photonuclear work in this nuclear mass region has been limited to a few experiments, from which can be derived information insufficient to answer the theoretical questions raised above. In particular, no systematic study of the osmium isotopes has been performed. Su Su *et al.*[14] have measured the photoneutron yield cross section $\sigma[(\gamma, 1n) + 2(\gamma, 2n) + 3(\gamma, 3n)]$ for natural osmium up to 27 MeV with a continuous bremsstrahlung radiation source and have attempted to extract the total photoneutron cross section $\sigma(\gamma, n_t) = \sigma[(\gamma, 1n) + (\gamma, 2n) + (\gamma, 3n)]$ from their yield data. Goryachev *et al.*[15] have measured the neutron yield cross sections for ^{184}W, ^{186}W, ^{185}Re, ^{187}Re, and ^{190}Os up to 20 MeV and have attempted to extract $\sigma(\gamma, n_t)$, also with a bremsstrahlung source, and using a rather impure (78.5%) sample for the ^{190}Os measurement. In addition to these two experiments, photonuclear measurements which used monoenergetic photons and neutron multiplicity counting to give the partial photoneutron cross sections $\sigma(\gamma, 1n) = \sigma[(\gamma, n) + (\gamma, pn)]$, $\sigma(\gamma, 2n) = \sigma[(\gamma, 2n) + (\gamma, p2n)]$, and $\sigma(\gamma, 3n)$, and hence $\sigma(\gamma, n_t)$, simultaneously and independently, have been carried out up to 29 MeV for ^{186}W as part of a larger study at this laboratory of the GDR in deformed nuclei,[16] and up to 22 MeV for natural samples of tungsten, rhenium, iridium, and platinum at Saclay.[17] Comparing these measurements with each other (insofar as is possible) yields good overall agreement between the results for ^{186}W of Refs. 15 and 16 and moderate agreement between the results of Ref. 15 for ^{185}Re and ^{187}Re and the results of Ref. 17 for natural rhenium. Since the measurement of Ref. 14 was done using natural osmium, it does not yield information on the evolution of the GDR or the GQR, but the results of Ref. 14 do show three rather spectacular peaks above the GDR, centered at about 19, 21, and 24 MeV. Since the existence of these peaks in $\sigma(\gamma, n_t)$ for *natural* osmium would favor *no* evolution of the GQR across this transitional mass region, it is important to see if this structure stands up to further experimental scrutiny. The data of Ref. 15 indicate less splitting of the GDR for ^{190}Os than for the other nuclei studied in that work, but the fact that $\sigma(\gamma, 2n)$ had to be estimated from a calculation in order to obtain $\sigma(\gamma, n_t)$ from the yield cross section makes this evidence for a possibly asymmetric or γ-unstable configuration for ^{190}Os somewhat tenuous. Of the nuclei studied in Refs. 16 and 17, it is clear that the tungsten and rhenium nuclei are prolate, but the evidence for the iridium and platinum nuclei is ambiguous, owing to the lack of measurements with isotopically enriched samples. Finally, the results of Ref. 16 yield a very small value for R_A (= 0.28) for ^{186}W, unlike nuclei which have larger static prolate deformations, which in turn calls into question one of the assumptions of the hydrodynamic model[3] used to interpret the data. It therefore would be interesting to delineate the behavior of R_A for the transitional osmium isotopes in order to explore further this hydrodynamic assumption, namely, that the Thomas-Reiche-Kuhn (TRK) sum rule is independent of the nuclear orientation (and hence of the nuclear radius); a proper quantum-mechanical description based upon a reasonable radial wave function might not require this condition. (Another quantitative test of this assumption is implicit in the photoneutron data for polarized ^{165}Ho of Kelly *et al.*[18] who found a two-standard-deviation departure from theoretical predictions for the asymmetry of the components of the GDR obtained with the ^{165}Ho nuclei aligned parallel and perpendicular to the photon beam direction.)

It should be noted that the two-resonance hydrodynamic model applies strictly only to nuclei having large permanent deformations. It will be seen below that the ^{190}Os and ^{192}Os nuclei probably are described better as vibrational rather than as rotational, and thus would have little or no ground-state equilibrium deformation. Consequently, the

area ratios mentioned above need not be 0.5 as predicted for statically deformed nuclei, and the quadrupole moments calculated from GDR parameters can be interpreted only as a measure of the average deformation of these nuclei.

An extensive discussion of most of these topics can be found in a recent review article[19]; the reader is referred there for amplification of many of the above points, together with discussion of relevant theoretical and experimental work from earlier literature in the field. The present measurements, then, were undertaken in order to throw light on these interesting questions of the possibility and characteristics of a phase transition, the evolution of the shapes of the GDR and GQR across the transitional mass region, and the delineation of the parameters relevant to the hydrodynamic interpretation of the GDR there.

II. EXPERIMENT AND DATA REDUCTION

The photoneutron measurements reported here were carried out with the monoenergetic photon beam obtained from the annihilation in flight of fast positrons from the Lawrence Livermore Laboratory Electron Positron Linear Accelerator facility. The photoneutrons were detected with an efficient paraffin-and-BF_3-tube 4π neutron detector.

The main features of the experimental techniques and data-reduction procedures have been given elsewhere in the literature, most recently in Ref. 20, where an extensive exposition includes a number of important changes made over the last few years. Therefore only those details peculiar to the present measurements will be given here.

The ring-ratio technique, whereby the average energy for the photoejected neutrons is determined for each data point, has for this work been extended to include triple-photoneutron events as well as single- and double-photoneutron events as in earlier work. These energies not only are of interest in themselves, but also serve to determine the neutron detector efficiencies necessary to compute the $(\gamma, 1n)$, $(\gamma, 2n)$, and $(\gamma, 3n)$ cross sections individually. Although the fractional uncertainties involved in the various partial cross sections might become appreciable in those energy regions where those cross sections themselves are small [such as for the $(\gamma, 1n)$ cross sections a few MeV above the $(\gamma, 2n)$ thresholds], owing to the statistical nature of ring-ratio data, the overall uncertainty in the total photoneutron cross section $\sigma(\gamma, n_t)$ is not much worsened by the imperfect knowledge of the detector efficiency (compared with the ~5% uncertainty in the photon flux calibration or the 2-to-4 % uncertainty in the electron-to-positron normalization factor, whose knowledge is necessary in order to subtract properly the photoneutron yield which results from positron bremsstrahlung). Thus, while the absolute cross sections have been determined with an accuracy of about 7%, the relative precision of the cross-section measurements between different osmium isotopes, [except possibly for ^{186}Os (see below)] is far better (2% to 3%).

The photon energy resolution for the present measurements varied from less than 250 keV at energies below 15 MeV to about 300 keV at 30 MeV. The absolute energy scale is known to within 0.25%. This was set with respect to the 15.11-MeV peak in the $^{13}C(\gamma, n)$ cross section,[21] and to many $(\gamma, 2n)$ threshold energies. The threshold values for the various photoneutron reactions for osmium isotopes are given in Table I (taken from Ref. 22), and are shown in the data plots by arrows. The threshold energies determined in the present measurements all agree, within the experimental limits, with the values tabulated in Ref. 22.

The sample specifications are given in Table II. All were in the form of powdered metal, packaged in an inert-gas atmosphere. The (large) samples of ^{188}Os, ^{189}Os, ^{190}Os, and ^{192}Os were contained in thin-walled lucite containers, and were run sequentially with the use of a pneumatic eight-position sample changer so that the beam-tuning conditions did not change between runs at a given energy for each sample. Sequential runs with an empty lucite container were performed as well for certain relevant energies (mainly in the giant-resonance region of the carbon and oxygen in the lucite). Also, at every energy a run was per-

TABLE I. Photoneutron threshold energies in MeV, from Ref. 22.

Nucleus	$E_{thr}(\gamma, n)$	$E_{thr}(\gamma, pn)$	$E_{thr}(\gamma, 2n)$	$E_{thr}(\gamma, p2n)$	$E_{thr}(\gamma, 3n)$
^{186}Os	8.271	14.156	14.896	20.627	23.706
^{188}Os	7.989	14.576	14.282	20.755	22.553
^{189}Os	5.924	13.133	13.913	20.500	20.206
^{190}Os	7.793	15.054	13.717	20.926	21.706
^{192}Os	7.558	15.718	13.318	21.337	21.111

TABLE II. Osmium sample specifications.

Nucleus	Mass (g)	Purity (%)	Principal impurities (%)
^{186}Os	3.28	78.2	^{188}Os 5.1
			^{189}Os 4.1
			^{190}Os 5.2
			^{192}Os 5.7
^{188}Os	22.49	94.5	^{189}Os 2.8
^{189}Os	30.94	94.5	^{190}Os 3.3
^{190}Os	49.70	97.8	
^{192}Os	83.51	99.1	

formed with the ^{190}Os sample in place in the center of the 4π neutron detector but with the 0.76-mm-thick beryllium annihilation target removed, so that the data can be corrected not only for cosmic-ray backgrounds, but also for those which are present when the accelerator is on but which are not connected with the annihilation-photon beam itself. For the ^{188}Os, ^{189}Os, and ^{192}Os samples these annihilation-target-out backgrounds were scaled according to mass, since the total photoneutron cross sections are roughly the same for all these nuclei. In any case, all these backgrounds were small compared with the counting rates for these large samples.

For ^{186}Os, although similar procedures were followed, the quality and quantity of data are not as good as for the other samples, for four reasons. First, the sample mass (3 g) was much smaller than the rest, which resulted in poorer counting statistics, even though longer runs were made for this isotope. Second, this sample was packaged in a small beryllium can, which necessitated separate sample-blank runs with another (empty) beryllium can, and separate annihilation-target-out runs, which were performed at every second energy (the results were interpolated for the intermediate energies). The relatively large mass (2 g) of the beryllium can and the resulting large sample-blank background would have made it very hard to obtain meaningful data for ^{186}Os above 20 MeV (the upper-energy limit of the present measurement for this sample), where the rise of the GDR of ^{9}Be takes place. Thus the statistical quality of the ^{186}Os data is limited further, particularly above about 18 MeV. Third, the ^{186}Os data were acquired at a different time from the rest of the data; and although a few runs also were performed with a similarly-packaged sample of ^{190}Os as a check on the absolute accuracy of the ^{186}Os data, another (probably small) uncertainty is thereby introduced. Fourth, the relatively low isotopic purity (see Table II) of 78% for the ^{186}Os sample necessitated appreciable corrections to the ^{186}Os cross sections [particularly to $\sigma(\gamma, 2n)$]. Of course, corrections for the known cross contamination of the cross-section data for all the osmium samples were made, and the resulting cross sections given in Sec. III below should be appropriate to samples of $100 \pm 0.1\%$ purity; nevertheless, this correction for the ^{186}Os case introduces another (again probably small) uncertainty. All in all, while the cross sections for the other osmium isotopes are accurate to about 7%, the ^{186}Os data cannot be said to be accurate to better than about 10%; and whereas the relative precision of the cross sections for the other osmium data is no worse than 2 to 3%, that for the ^{186}Os data with respect to the others might very well be as large as 5%.

The data-reduction procedures incorporated the recent improvements discussed at some length in Ref. 20, whereby each step in the data reduction is handled in modular fashion, with human interaction with the computer used where such interaction results in more accurate results. These steps are corrections for pileup, corrections for drift of the neutron detector and of the ionization chamber which is the photon beam monitor (done with the aid of calibration runs made with radioactive neutron and γ-ray sources at frequent intervals throughout the experiment), subtraction of the various backgrounds, including the contribution of the positron bremsstrahlung, use of the ring-ratio data to obtain the detector efficiency for each neutron multiplicity as a function of photon energy, use of the efficiencies so derived to determine the final photoneutron multiplicities, and final conversion of the photoneutron yield data to cross sections, taking into account the annihilation photon flux calibration, the solid angles involved, the number of atoms in the sample under study (that are bathed in the photon beam), and the attenuation of the photon beam in passing through the sample. All the uncertainties that play any significant role in the final results of Sec. III below already have been discussed above; for further details regarding experimental techniques and data-reduction procedures, the reader is referred to Ref. 20.

III. RESULTS AND DISCUSSION

A. Average photoneutron energies

The average neutron energies for $(\gamma, 1n)$, $(\gamma, 2n)$, and $(\gamma, 3n)$ events (except for ^{186}Os) derived from the ring-ratio data are shown in Fig. 1 as functions of photon energy. These data are in the form of solid lines, which represent the actual data in the energy regions where they are statistically sound. Of course, ring-ratio data were obtained for all neutron multiplicities measured, for all energies

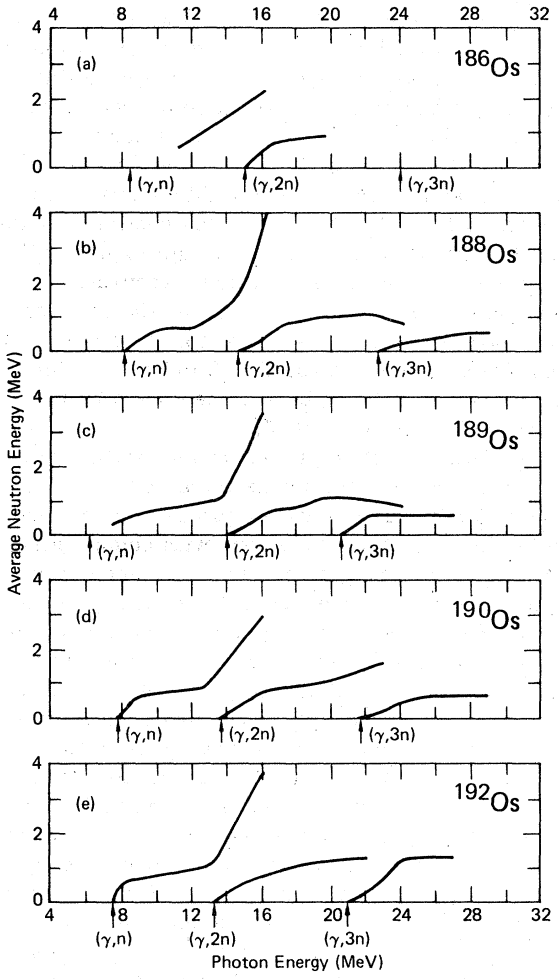

FIG. 1. Average photoneutron energies plotted as functions of photon energy: (a) $(\gamma,1n)$ and $(\gamma,2n)$ channels for ^{186}Os; (b) $(\gamma,1n)$, $(\gamma,2n)$, and $(\gamma,3n)$ channels for ^{188}Os; (c) the same as (b) for ^{189}Os; (d) the same as (b) for ^{190}Os; (e) the same as (b) for ^{192}Os.

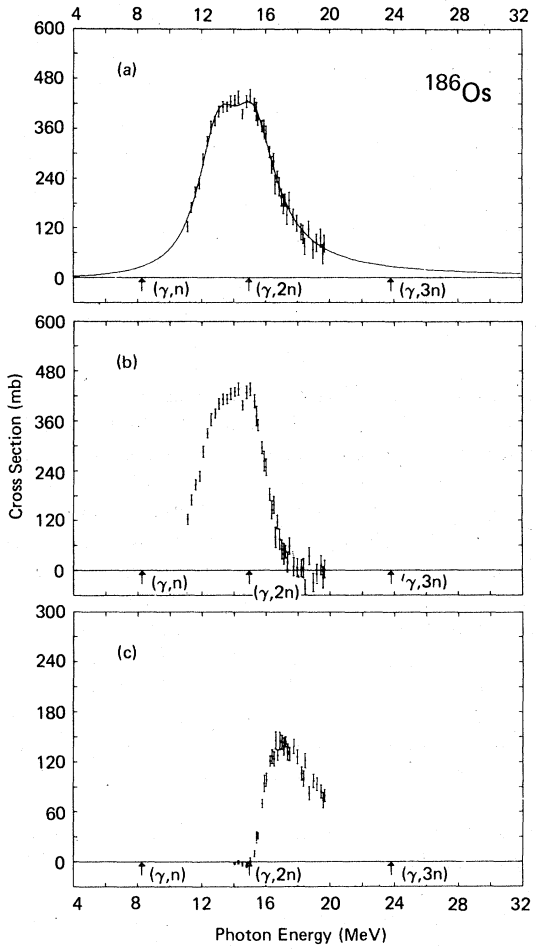

FIG. 2. Photoneutron cross sections for ^{186}Os: (a) total photoneutron cross section $\sigma(\gamma,n_i)=\sigma[(\gamma,1n)+(\gamma,2n)]$, together with a two-component Lorentz-curve fit to the data (solid line); (b) single-photoneutron cross section $\sigma(\gamma,1n)=\sigma[(\gamma,n)+(\gamma,pn)]$; (c) double-photoneutron cross section $\sigma(\gamma,2n)$.

above their thresholds up to the maximum photon energy used for each isotope, and in fact these data were used to determine the neutron detector efficiencies as outlined in Sec. II above. However, the statistical quality of the ring-ratio data in energy regions where the partial cross sections are small is such that (even though no major uncertainties in the data are produced) little useful (from the nuclear-physics point of view) average-neutron-energy information is obtained there. These energy regions lie above about 16 MeV for $(\gamma,1n)$ data, above 22–24 MeV for $(\gamma,2n)$ data, and above 27–29 MeV for $(\gamma,3n)$ data.

There are a few features of the average neutron energies that all the osmium nuclei appear to have in common. First, the average (single) photoneutron energy at the photon energy corresponding to the lower-energy peak of a two-component Lorentz-curve fit to the GDR (see below), which varies from 12.7 to 13.0 MeV, is close to 1.0 MeV. Second, the average single-photoneutron energy rises rapidly above the $(\gamma,2n)$ threshold. This can be understood as resulting simply from the opening of the $(\gamma,2n)$ decay channel, which bleeds off the events characterized by low-energy photoneutrons. Third, the average neutron energies for $(\gamma,2n)$ and $(\gamma,3n)$ events approach roughly asymptotic values at energies sufficiently far (typically a few MeV) above their thresholds. For the $(\gamma,2n)$ channel these values are not far from 1 MeV (for ^{190}Os, it appears from Fig. 1 that the average double-photoneutron energy still is rising

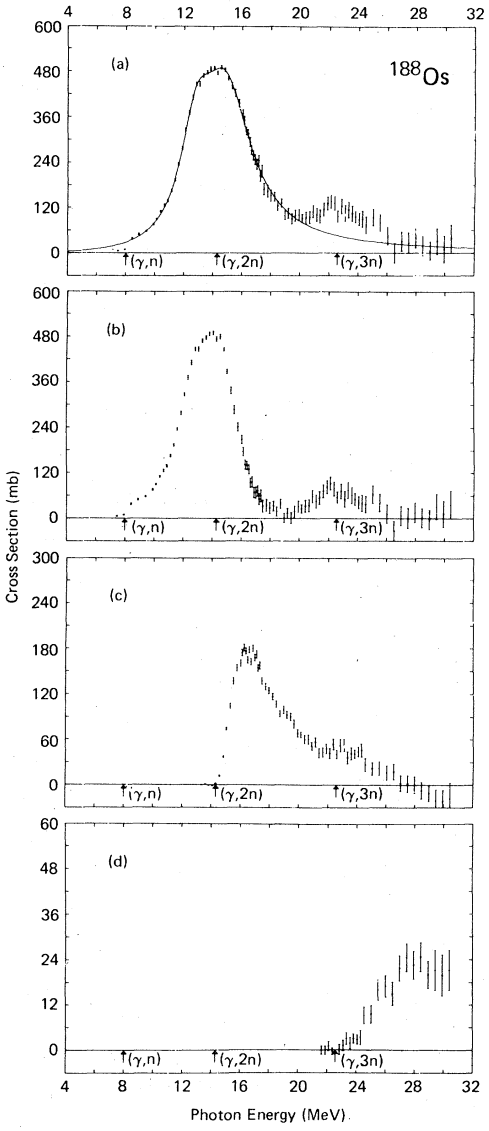

FIG. 3. Photoneutron cross sections for ^{188}Os: (a) $\sigma(\gamma, n_t)$, with a two-component Lorentz-curve fit; (b) $\sigma(\gamma, 1n)$; (c) $\sigma(\gamma, 2n)$; (d) triple-photoneutron cross section $\sigma(\gamma, 3n)$.

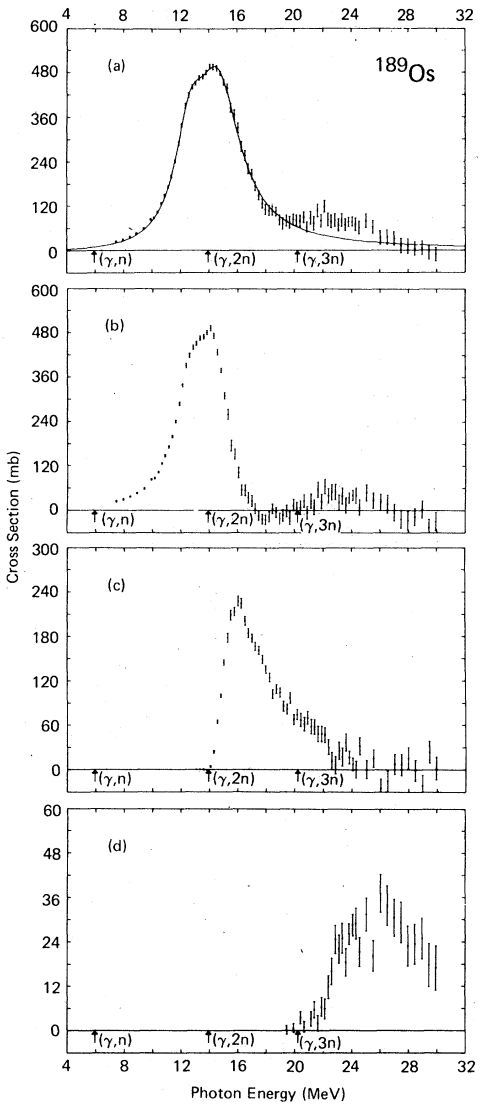

FIG. 4. Photoneutron cross sections for ^{189}Os: (a) $\sigma(\gamma, n_t)$, with a two-component Lorentz-curve fit; (b) $\sigma(\gamma, 1n)$; (c) $\sigma(\gamma, 2n)$; (d) $\sigma(\gamma, 3n)$.

slowly at 23 MeV, but it decreases somewhat at still higher energies); for the $(\gamma, 3n)$ channel the value for ^{192}Os is above 1 MeV, while for the other three [no $(\gamma, 3n)$ data were obtained for ^{186}Os] these values are about 0.6 MeV.

B. Cross sections

The photoneutron cross sections for ^{186}Os, ^{188}Os, ^{189}Os, ^{190}Os, and ^{192}Os are shown as functions of photon energy in Figs. 2–6, respectively. The total photoneutron cross sections [part (a) of the figures] all have about the same peak height, except that for ^{186}Os, which is ~10% smaller than the rest (but see the *caveat* regarding the ^{186}Os data in Sec. II above). On the other hand, the GDR for ^{186}Os is a bit broader than the rest, and there is a gradual decrease both in the width of the flattened region at the peak and in the overall width of the GDR. A broad peak, centered at about 23 MeV, appears in $\sigma(\gamma, n_t)$ for all cases where the data include this energy region. This peak is most prominent for ^{188}Os, where it is clearly present in both $\sigma(\gamma, 1n)$ [Fig. 3(b)] and in $\sigma(\gamma, 2n)$ [Fig. 3(c)];

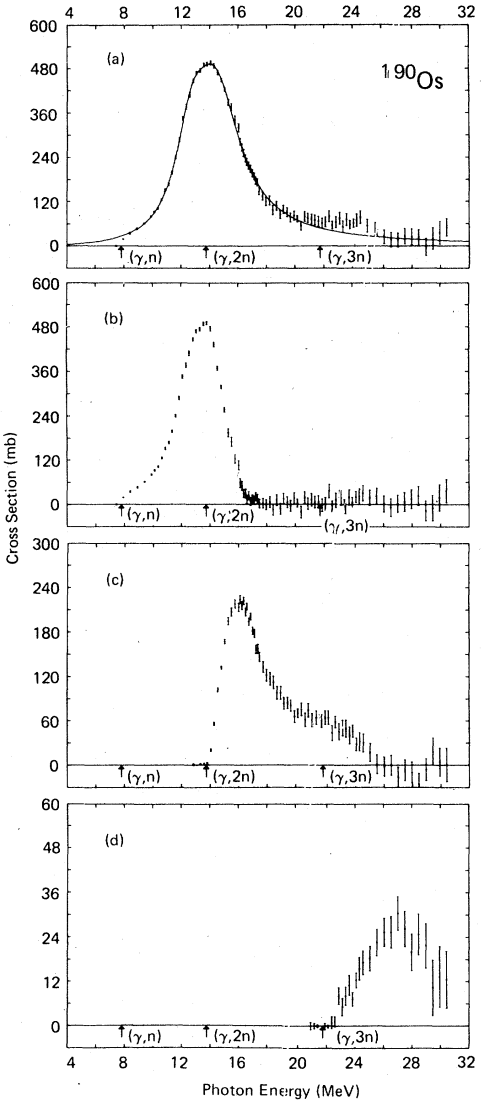

FIG. 5. Photoneutron cross sections for ^{190}Os: (a) $\sigma(\gamma, n_t)$, with a two-component Lorentz-curve fit; (b) $\sigma(\gamma, 1n)$; (c) $\sigma(\gamma, 2n)$; (d) $\sigma(\gamma, 3n)$.

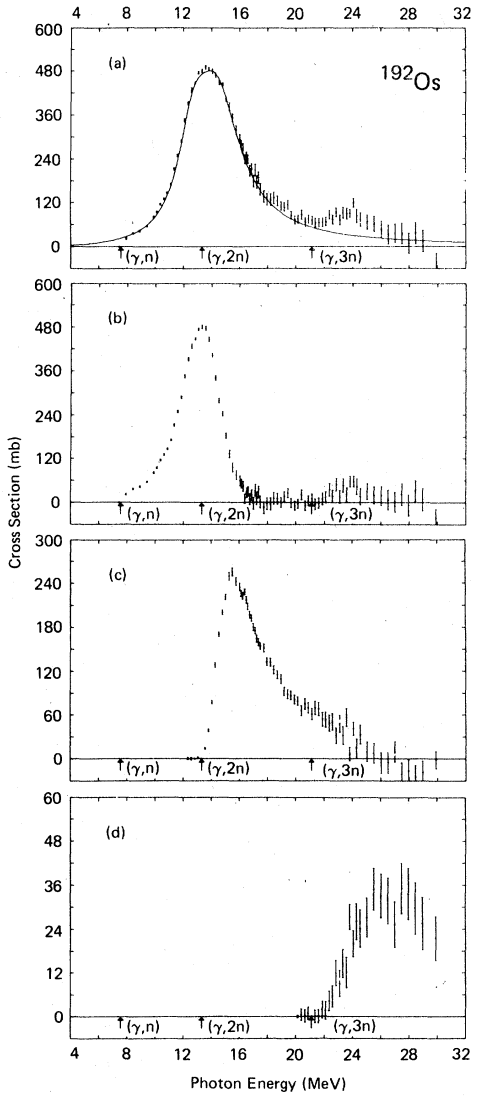

FIG. 6. Photoneutron cross sections for ^{192}Os: (a) $\sigma(\gamma, n_t)$, with a two-component Lorentz-curve fit; (b) $\sigma(\gamma, 1n)$; (c) $\sigma(\gamma, 2n)$; (d) $\sigma(\gamma, 3n)$.

it is least prominent for ^{190}Os, so that it is not the case that the strength of this high-energy resonance decreases systematically with increasing mass (or neutron number N). It should be noted that the presence of this resonance in the $(\gamma, 1n)$ cross sections might arise from strength in the (γ, pn) channel. (This channel would be largely suppressed by the Coulomb barrier for these high-Z nuclei at lower excitation energies.) The $(\gamma, 1n)$ cross sections [part (b) of the figures] all decrease rapidly to zero within a few (3 or 4) MeV of the $(\gamma, 2n)$ thresholds. Similar behavior has been observed for nearly every other medium or heavy nucleus studied at this laboratory[19] [an exception is ^{107}Ag (Ref. 23)], and can be understood on the basis of the usual statistical model, where the direct-reaction component of the GDR is small. This behavior also is seen here for the $(\gamma, 2n)$ cross sections [part (c) of the figures] just above the $(\gamma, 3n)$ thresholds. The $(\gamma, 2n)$ cross sections get larger rapidly as N increases and the $(\gamma, 2n)$ threshold decreases. This effect has been seen before, for example, for the zirconium isotopes,[24] and can be understood as resulting from the $(\gamma, 2n)$ threshold biting further into the GDR with increasing N. A similar but less pronounced effect can

TABLE III. Parameters of Lorentz-curve fits to the giant dipole resonance. Lorentz parameters defined by Eq. (1); the fitting interval for all cases is 10.8 to 18.8 MeV.

Nucleus	$E_m(1)$ (MeV)	$\sigma_m(1)$ [a] (mb)	$\Gamma(1)$ (MeV)	$E_m(2)$ (MeV)	$\sigma_m(2)$ [a] (mb)	$\Gamma(2)$ (MeV)	χ^2
^{186}Os	13.03 ± 0.09	308 ± 21	3.13 ± 0.24	15.26 ± 0.09	302 ± 23	3.38 ± 0.21	0.88
^{188}Os	12.81 ± 0.05	260 ± 18	2.76 ± 0.13	14.88 ± 0.07	390 ± 14	4.19 ± 0.13	0.96
^{189}Os	12.68 ± 0.04	268 ± 14	2.71 ± 0.10	14.68 ± 0.05	395 ± 11	3.62 ± 0.10	0.75
^{190}Os	12.68 ± 0.07	206 ± 29	2.60 ± 0.21	14.40 ± 0.09	401 ± 24	4.16 ± 0.11	1.19
^{192}Os	12.68 ± 0.06	206 ± 34	2.49 ± 0.23	14.35 ± 0.12	389 ± 26	4.41 ± 0.13	0.95

[a] Uncertainties for σ_m given here are relative. The absolute uncertainties are 7% (10% for ^{186}Os).

be seen for the $(\gamma, 3n)$ cross sections [part (d) of Figs. 3–6]. Again, as has been seen before for many medium and heavy nuclei,[19] the $(\gamma, 2n)$ cross sections rise steeply above their thresholds, but the $(\gamma, 3n)$ cross sections rise much more gradually above theirs.

Comparison of the present (γ, n_t) cross section for ^{190}Os with that of Ref. 15 reveals a considerable discrepancy, both in magnitude and shape. Comparison of the present $\sigma(\gamma, n_t)$ results with those for natural osmium of Ref. 14 reveals a similar discrepancy in magnitude (~15%); moreover, the high-energy structure that is so prominent in the results of Ref. 14, particularly the largest peak, at ~19 MeV, cannot be reconciled with that seen in the present work. Although the precise reasons for these discrepancies are not obvious, it should be noted again that the measurements of Ref. 14 and Ref. 15 both were performed with bremsstrahlung sources (and consequently with the usual unfolding difficulties), and neither made use of neutron multiplicity counting.

C. Giant-resonance parameters

The classic collective description of the GDR predicts that the total photon absorption cross section $\sigma(\gamma, \text{tot})$ for statically deformed spheroidal nuclei is characterized as the sum of two Lorentz-shaped curves,

$$\sigma(\gamma, \text{tot}) = \sum_{i=1}^{2}\left[\sigma_m(i)\Big/\left(1+\frac{[E_\gamma^{\,2}-E_m^{\,2}(i)]^2}{E_\gamma^{\,2}\Gamma^2(i)}\right)\right], \qquad (1)$$

where $\sigma_m(i)$, $E_m(i)$, and $\Gamma(i)$ are the peak height, resonance energy, and full width of the ith Lorentz curve. For medium-heavy nuclei (and certainly for the osmium isotopes, for which $Z = 76$), the Coulomb barrier greatly inhibits the emission of charged particles at giant-resonance energies, and the photon scattering cross section is always small above the (γ, n) threshold; therefore, the total photoneutron cross section $\sigma(\gamma, n_t)$ is an excellent approximation to $\sigma(\gamma, \text{tot})$. Accordingly, the (γ, n_t) cross sections in part (a) of Figs. 2–6 have been fitted with two-component Lorentz curves. The fitting interval used for all five nuclei was 10.8–18.8 MeV; as has been found in the past,[16,18,23,24] reasonable departures from this interval do not change the results appreciably (the present data were fitted for the intervals 11–17 and 11–18 MeV as well). The main reason that this particular fitting interval was chosen is that all the previous monoenergetic-photon data for deformed nuclei[16,19,25] have been analyzed in this fashion, and thus the use of this interval facilitates comparison. The resulting fits to the data are shown in part (a) of Figs. 2–6, and the Lorentz parameters of these fitted curves are given, together with their statistical uncertainties, in Table III; the χ^2 values[19] for these fits are given in the last column of the table.

In order to ascertain whether the shape of the GDR for the osmium isotopes could be approximated as well by a single Lorentz curve, as would be the case for spherical nuclei, the data were fitted with such curves. The results rebut emphatically any such sphericity for these nuclei: the χ^2 values for single-component Lorentz fits for the same fitting interval as above are 3.8, 13.7, 13.9, 8.0, and 9.4 for ^{186}Os, ^{188}Os, ^{189}Os, ^{190}Os, and ^{192}Os, respectively, far in excess of the χ^2 values for two-component Lorentz fits given in Table III. (The χ^2 value for ^{186}Os is as low as it is only because of the relatively poorer statistical quality of the data.) It is interesting, however, to note the significant difference between the situation for ^{188}Os and ^{189}Os and that for ^{190}Os and ^{192}Os. The former two nuclei have a GDR shape rather broader than that for the latter two, so that a single-component fit to the former yields χ^2 values significantly larger than a fit to the latter. This can be seen more clearly in Fig. 7, where these single-component Lorentz fits to $\sigma(\gamma, n_t)$ for ^{188}Os and ^{190}Os are shown, to be compared with each other and with the corresponding two-component fits shown in Figs. 3(a) and 5(a).

Values of the parameters for the classical theories are given in Table IV. These include α and β, the proportionality constants characterizing

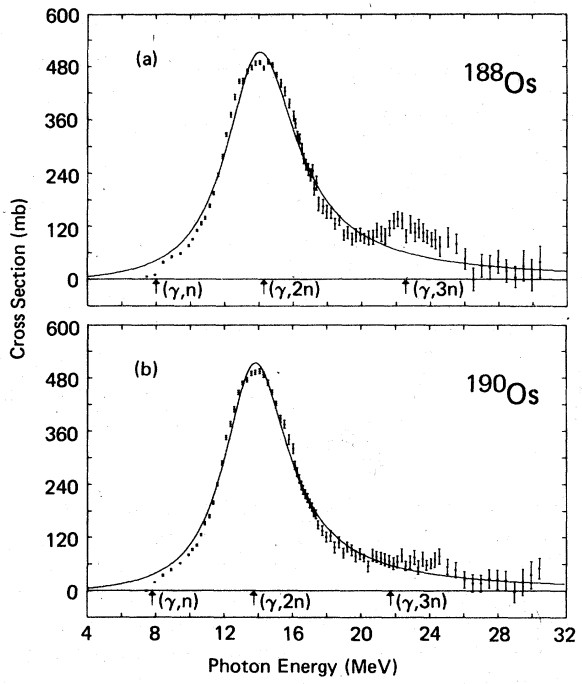

FIG. 7. Total photoneutron cross sections, together with single-component Lorentz-curve fits to the data: (a) for ^{188}Os; (b) for ^{190}Os.

the mean GDR energy E_m with mass number, and K, the nuclear symmetry energy computed from the relation[3]

$$K = 9.935\times10^{-4}\frac{A^{8/3}}{NZ}\frac{[E_m(1)]^2}{1-[\Gamma(1)/2E_m(1)]^2}\times\frac{\eta^{4/3}}{(1+0.018\,60\epsilon-0.033\,14\epsilon^2)^2}, \quad (2)$$

where η is the nuclear deformation parameter, defined as the ratio of the semimajor axis b to the semiminor axis a of the (prolate) deformed nucleus, and computed from the relation[3]

TABLE IV. Parameters for classical theories (given in MeV).

Nucleus	E_m [a]	α [b]	β [c]	K [d]
^{186}Os	14.21 ± 0.06	81.1 ± 0.3	34.0 ± 0.1	28.9 ± 0.9
^{188}Os	14.19 ± 0.05	81.3 ± 0.3	34.0 ± 0.1	27.8 ± 0.5
^{189}Os	14.01 ± 0.04	80.4 ± 0.2	33.6 ± 0.1	27.3 ± 0.4
^{190}Os	13.83 ± 0.06	79.5 ± 0.3	33.1 ± 0.1	26.6 ± 0.7
^{192}Os	13.79 ± 0.04	79.6 ± 0.2	33.1 ± 0.1	26.8 ± 0.7

[a] Mean energy of the giant resonance, defined as $E_m = [E_m(1) + 2E_m(2)]/3$, except for ^{186}Os, for which $E_m = [E_m(1) + E_m(2)]/2$.
[b] Hydrodynamic parameter, defined by $E_m = \alpha A^{-1/3}$.
[c] Collective parameter, defined by $E_m = \beta A^{-1/6}$.
[d] Nuclear symmetry energy, computed from Eq. (2).

$$E_m(2)/E_m(1) = 0.911\eta + 0.089, \quad (3)$$

and ϵ is the nuclear eccentricity, defined as $(b^2 - a^2)/R^2$, where R is the radius of a sphere of equal volume (for a prolate spheroid, $R^3 = a^2 b$), and computed from the resulting relation

$$\epsilon = (\eta^2 - 1)\eta^{-2/3}. \quad (4)$$

The value for E_m for a prolate spheroid should be given by

$$E_m = [E_m(1) + 2E_m(2)]/3, \quad (5)$$

two-thirds of the way from the lower- to the higher-energy peak of the GDR; this value has been adopted for all the osmium isotopes but ^{186}Os, for which a value for E_m midway between the two peaks of the GDR was adopted, because of the near equality of the strengths of the two Lorentz components for this nucleus. It can be seen from Table IV that this procedure results in values for E_m for ^{190}Os and ^{192}Os significantly lower than those for ^{186}Os and ^{188}Os, with that for ^{189}Os lying in between.

Values for various nuclear shape parameters, computed from the Lorentz parameters of Table

TABLE V. Nuclear shape parameters.

Nucleus	R_A [a]	η [b]	ϵ [c]	β_2 [d]	Q_0 [e] (b)
^{186}Os	0.95 ± 0.27	1.188 ± 0.016	0.366 ± 0.031	0.194 ± 0.016	5.76 ± 0.49
^{188}Os	0.44 ± 0.08	1.177 ± 0.011	0.346 ± 0.021	0.183 ± 0.011	5.49 ± 0.33
^{189}Os	0.51 ± 0.07	1.173 ± 0.008	0.338 ± 0.015	0.179 ± 0.008	5.38 ± 0.24
^{190}Os	0.32 ± 0.10	1.149 ± 0.015	0.292 ± 0.029	0.155 ± 0.015	4.65 ± 0.46
^{192}Os	0.30 ± 0.11	1.145 ± 0.016	0.283 ± 0.031	0.150 ± 0.016	4.55 ± 0.50

[a] Area ratio, defined as $\sigma_m(1)\Gamma(1)/\sigma_m(2)\Gamma(2)$.
[b] Deformation parameter, computed from $E_m(2)/E_m(1) = 0.911\eta + 0.089$.
[c] Nuclear eccentricity, computed from $\epsilon = (\eta^2 - 1)\eta^{-2/3}$.
[d] Deformation parameter, defined as $\frac{2}{3}(\pi/5)^{1/2}\epsilon$.
[e] Intrinsic quadrupole moment, computed from Eq. (8), with R_0 taken to be 1.26 fm.

TABLE VI. Values for $B(E2, 0^+ \rightarrow 2^+)$ (in units of b^2).

Nucleus	Present experiment [a]	μ-mesic x rays [b]	Coulomb excitation [c]	Theory [d]	Theory [e]
^{186}Os	3.30 ± 0.56	3.15 ± 0.03	3.08 ± 0.21	2.96	3.05
^{188}Os	3.00 ± 0.36	2.84 ± 0.03	2.75 ± 0.12	2.72	2.75
^{190}Os	2.15 ± 0.43	2.48 ± 0.02	2.40 ± 0.11	2.59	2.54
^{192}Os	2.06 ± 0.46	2.10 ± 0.02	2.02 ± 0.09	2.56	2.34

[a] Computed from Eq. (9), using the values for Q_0 from Table V.
[b] From Ref. 26.
[c] Weighted average from Refs. 27 and 28.
[d] From Ref. 5.
[e] From Ref. 6.

III, are given in Table V. These are R_A, the area ratio defined as

$$R_A = \sigma_m(1)\Gamma(1)/\sigma_m(2)\Gamma(2) \quad (6)$$

and predicted to be one-half for prolate nuclei; η, the deformation parameter of Eq. (3); ϵ, the nuclear eccentricity of Eq. (4); β_2, a deformation parameter more commonly used than η or ϵ, defined as

$$\beta_2 = \tfrac{2}{3}(\pi/5)^{1/2}\epsilon \simeq 0.53\epsilon\,, \quad (7)$$

and Q_0, the intrinsic quadrupole moment defined as

$$Q_0 = \tfrac{2}{5}ZR^2\epsilon\,, \quad (8)$$

where the equivalent nuclear radius $R = R_0A^{1/3}$, and R_0 is here taken to be 1.26 fm, in keeping with the results of Ref. 16. (It should be noted that the photonuclear approach yields the eccentricity ϵ of the nuclear matter distribution while the Coulomb-excitation approach yields a parameter which describes the shape of the charge distribution.)

From the values in Table V, a substantial and significant difference is obtained between the nuclear shape parameters for ^{188}Os and ^{189}Os on the one hand and for ^{190}Os and ^{192}Os on the other. (The value for R_A for ^{186}Os is large and uncertain, so that it would be rash to place very much credence in its value, particularly in view of the statistical uncertainties in the ^{186}Os data discussed in Sec. II above; the values for ^{186}Os for the other quantities in Table V seem reasonable enough, however.) The values of R_A for ^{188}Os and ^{189}Os are, within the statistical uncertainty of the data, equal to the value of 0.5 characteristic of statically deformed prolate nuclei, while the values of R_A for ^{190}Os and ^{192}Os differ from 0.5 by about two standard deviations. Likewise, the values of the other quantities listed in Table V (which, of course, are related to each other) for ^{188}Os and ^{189}Os again differ from those for ^{190}Os and ^{192}Os by about two standard deviations.

In Table VI are given the values for $B(E2, 0^+ \rightarrow 2^+)$, the electric-quadrupole transition probability computed from the usual relationship that applies to rotational nuclei

$$Q_0^2 = (16\pi/5)B(E2, 0^+ \rightarrow 2^+)\,, \quad (9)$$

and is used frequently in Coulomb-excitation or μ-mesic x-ray studies to deduce the magnitude (but not the sign) of Q_0 for even-even nuclei. It is noted in passing that Eqs. (7), (8), and (9) can be combined to give

$$[B(E2)]^{1/2} = (3/4\pi)ZR^2\beta_2\,. \quad (10)$$

Also given in this table are the corresponding $B(E2)$ values from other experiments as well as those from the theoretical calculations of Refs. 5 and 6. It is seen that the present data agree better with other experimental work than with either theoretical calculation, and that the calculation of Ref. 6, because it predicts a larger range of values

TABLE VII. Various theoretical predictions for nuclear shape parameters.

Nucleus	β_2 (Ref. 29) ($\beta_4 \neq 0$)	β_2 (Ref. 29) ($\beta_4 = 0$)	β_2 (Ref. 30)	Q_0 (Ref. 31) (b) ($Q_4 \neq 0$)	β_2 (Ref. 32) ($\beta_4 \neq 0$)	Q_0 (Ref. 32) (b) ($Q_4 \neq 0$)
^{186}Os	0.22	0.19	0.214	6.01	0.202	4.26
^{188}Os	0.20	0.17	0.197	5.55	0.202	4.26
^{189}Os				5.24		
^{190}Os	0.18	0.16	0.180	4.73	−0.266	−6.33
^{192}Os	0.17	0.14	0.158	4.44	−0.253	−5.91

TABLE VIII. Parameters of three-component Lorentz-curve fits to the GDR. See text for the explanation of the constraints on these fits.

Nucleus	E_1 (MeV)	E_2 (MeV)	E_3 (MeV)	χ^2
^{186}Os	12.86±0.07	14.21±0.22	15.45±0.09	0.82
^{188}Os	12.84±0.03	14.68±0.13	15.28±0.22	0.97
^{189}Os	12.66±0.02	14.35±0.10	15.03±0.13	0.69
^{190}Os	12.77±0.04	14.34±0.11	14.94±0.21	1.25
^{192}Os	12.75±0.03	14.31±0.07	15.16±0.19	0.93

for $B(E2)$ over the span of the osmium isotopes than that predicted by the calculation of Ref. 5, matches all the experimental data somewhat better than that of Ref. 5.

A number of other theoretical calculations have been performed recently, whose results, listed in Table VII, can be compared to the present experimental results (Table V). Götz *et al.*,[29] who first discussed the significance of including hexadecapole deformations in describing the osmium isotopes, obtained values for β_2 which agree better with the present results when the hexadecapole deformations β_4 are ignored than when they are included; they also obtain a prolate-oblate phase transition at $A \sim 192$. Gabrakov *et al.*[30] used the method of summation of the single-particle energy levels to obtain values for β_2 in fair agreement with the present results; they also predict a prolate-oblate phase transition, but at $N = 108$ (^{184}Os). Ekström *et al.*[31] employed a Nilsson-model (a modified oscillator model) calculation to find minima in the potential-energy surfaces, which in turn yield equilibrium quadrupole and hexadecapole deformations; their results represent a substantial improvement upon those of Ref. 29 in that they obtain quite remarkable agreement with the present results (they give their results in terms of the intrinsic quadrupole moments) at the same time that they include the hexadecapole effects (and moreover, they obtain results for the odd-A nucleus ^{189}Os as well). Finally, Goss,[32] using a self-consistent version of the anisotropic oscillator model, obtains triaxial shapes for the even-A osmium nuclei, for which the values for β_2 (and Q_0) change sign between ^{188}Os and ^{190}Os, contrary to the present results; in other words, he has got the wrong thing happening at the right place (see Sec. III G below).

An alternative approach to fitting the GDR data for these nuclei, where there is no distinct splitting into two well-separated peaks, is to fit the data with three (overlapping) Lorentz curves. In order to do this in a mathematically reasonable way, however, it is necessary to reduce the number of arbitrary parameters from nine, to (say) six. If any physical meaning is to be attached to the results (in terms of a triaxial model), the three resonance energies must be allowed to vary. We therefore imposed the conditions that each of the three Lorentz components have equal strength (corresponding to the assumption that the dipole sum rule holds for vibrations along each nuclear axis separately) and that the total strength be equal to that found for the corresponding two-component Lorentz fit (a normalization condition). The fits resulting from this procedure were approximately as good as for the two-component case; the resulting resonance energies and χ^2 values are given in Table VIII. These energies then can be used to infer the nuclear shape, since in this naive model they are inversely proportional to the lengths of the three nuclear axes. Thus it can be said that if a rigid triaxial picture for these nuclei has any validity, then the shape asymmetry should be given by the ratios of these energies.

D. Integrated cross sections

The integrated cross sections measured in this work are summarized in Table IX. Columns 3, 4, and 5 in this table list the integrated single-, double-, and triple-photoneutron cross sections, respectively; column 6 lists the ratio of the in-

TABLE IX. Integrated cross sections, $\sigma_{\rm int}(\gamma,x) = \int \sigma(\gamma,x)dE_\gamma$, integrated from threshold to $E_{\gamma\max}$. Uncertainties are discussed in Sec. II of the text.

Nucleus	$E_{\gamma\max}$ (MeV)	$\sigma_{\rm int}(\gamma,1n)$ (MeV b)	$\sigma_{\rm int}(\gamma,2n)$ (MeV b)	$\sigma_{\rm int}(\gamma,3n)$ (MeV b)	$\frac{\sigma_{\rm int}(\gamma,2n)}{\sigma_{\rm int}(\gamma,n_t)}$	$\frac{\sigma_{\rm int}(\gamma,n_t)}{0.06NZ/A}$	$\frac{\frac{1}{2}\pi[\sigma_m(1)\Gamma(1)+\sigma_m(2)\Gamma(2)]}{0.06NZ/A}$ [a]
^{186}Os	19.67 [b]	2.04	0.46	...	0.19	0.93±0.09	1.15±0.12
^{188}Os	30.42	2.62	0.88	0.12	0.24	1.33±0.09	1.36±0.08
^{189}Os	29.92	2.13	1.00	0.21	0.30	1.23±0.09	1.24±0.06
^{190}Os	30.42	2.01	1.08	0.14	0.33	1.18±0.08	1.27±0.10
^{192}Os	29.92	1.92	1.20	0.19	0.36	1.20±0.08	1.27±0.11

[a] Uncertainties listed here are relative; to obtain the absolute uncertainty a systematic uncertainty of 7% (10% for ^{186}Os) must be folded into the values for σ_m.

[b] Care must be used comparing values for ^{186}Os with the rest because $E_{\gamma\max}$ is so much different.

TABLE X. Integrated cross-section moments, $\sigma_{-1}=\int\sigma(\gamma,n_t)E_\gamma^{-1}dE_\gamma$ and $\sigma_{-2}=\int\sigma(\gamma,n_t)E_\gamma^{-2}dE_\gamma$, integrated from threshold to $E_{\gamma\max}$.

Nucleus	σ_{-1} (mb)	$\sigma_{-1}A^{-4/3}$ (mb)	σ_{-2} (mb MeV^{-1})	$\frac{\sigma_{-2}}{0.00225A^{5/3}}$	$\frac{\sigma_{-2}K}{0.05175A^{5/3}}$	$\frac{0.05175A^{5/3}}{\sigma_{-2}}$ (MeV)
^{186}Os[a]	179	0.168	13.2	0.97	1.22	23.8±2.4
^{188}Os	239	0.222	16.7	1.20	1.45	19.1±1.3
^{189}Os	228	0.210	16.7	1.19	1.41	19.3±1.4
^{190}Os	220	0.202	15.8	1.12	1.30	20.6±1.4
^{192}Os	224	0.203	16.0	1.12	1.31	20.6±1.4

[a] Care must be used in comparing values for ^{186}Os with the rest because $E_{\gamma\max}$ is so much different.

tegrated double to total photoneutron cross sections; column 7 lists the measured integrated total photoneutron cross section in TRK sum-rule units; and column 8 lists the total area under the two-component Lorentz-curve fits to $\sigma(\gamma,n_t)$ in those units. The values listed in columns 7 and 8 give an indication of the maximum amount of exchange-force enhancement of the dipole sum-rule values that might be needed to account for the GDR, and are consistent with, albeit somewhat larger than, the mean of many measurements on other nuclei made with monoenergetic photons.[19,25]

The integrated moments of the measured total photoneutron cross sections σ_{-1} and σ_{-2} are given in columns 2 and 4, respectively, of Table X. Migdal[33] derived a sum rule for σ_{-2} based upon the assumption of a constant nuclear (but variable neutron and proton) density. The value of σ_{-2}, which is proportional to the nuclear polarizability, is predicted to be[34]

$$\sigma_{-2}=0.05175A^{5/3}/K \text{ mb MeV}^{-1} \qquad (11)$$

for spherical nuclei, where K is in MeV and $R_0=1.20$ fm; for $K=23$ MeV, $\sigma_{-2}=0.00225A^{5/3}$ mb MeV^{-1}. It can be seen from column 5 of Table IX that the experimental values lie within 20% of this prediction. If instead of the constant 23 MeV, however, the values for K given in Table IV are used, column 6 of Table X shows that the agreement for this case is not nearly as good. Indeed, the values of the nuclear symmetry energy computed from the values for σ_{-2} by use of Eq. (11), listed in the last column of Table X differ from those in Table IV by an average of 33%. Since such a discrepancy is not observed for nuclei which have no equilibrium deformation,[12,23,24] where the two methods for computing K yield essentially the same results, the discrepancy observed here can be taken to indicate that the osmium nuclei are statically deformed. It should be noted once again that there is an appreciable difference between ^{188}Os and ^{189}Os, for which the difference between symmetry energies computed

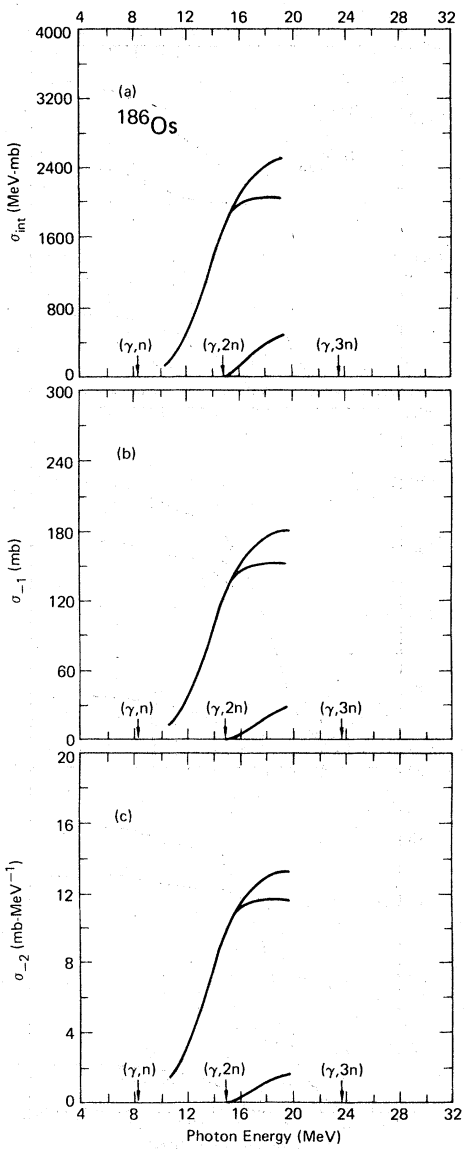

FIG. 8. Running sums of integrated photoneutron cross sections and their moments for ^{186}Os: (a) $\sigma_{\rm int}=\int\sigma dE_\gamma$ for $\sigma(\gamma,n_t)$ (top), $\sigma(\gamma,1n)$ (middle), and $\sigma(\gamma,2n)$ (bottom); (b) $\sigma_{-1}=\int\sigma E_\gamma^{-1}dE_\gamma$; (c) $\sigma_{-2}=\int\sigma E_\gamma^{-2}dE_\gamma$.

in these two ways is over 8 MeV, and ^{190}Os and ^{192}Os, for which this difference is about 6 MeV. This again indicates that the former are more deformed than the latter, in agreement with the results given in Tables V and VI.

The present experimental data on all the integrated cross sections and their moments are shown in Figs. 8–12, in the form of running sums of the quantities plotted as functions of the photon energy up to which they are integrated. This form of displaying the integrated cross-section data is useful for information-retrieval purposes, and also shows whether and how well the various plotted quantities approach asymptotic behavior at high photon energies. These figures show that the integrated cross sections (and their moments) do indeed approach asymptotic values [except for the $(\gamma, 3n)$ reactions] by 30 MeV, and hence, if there is no further prominent structure in the cross sections at energies higher than this, make possible reasonable extrapolations to higher energies. [Of course, high-multiplicity cross sections, such as $(\gamma, 4n)$, will play a role at these higher energies (see, for example, Refs. 35 and 36).]

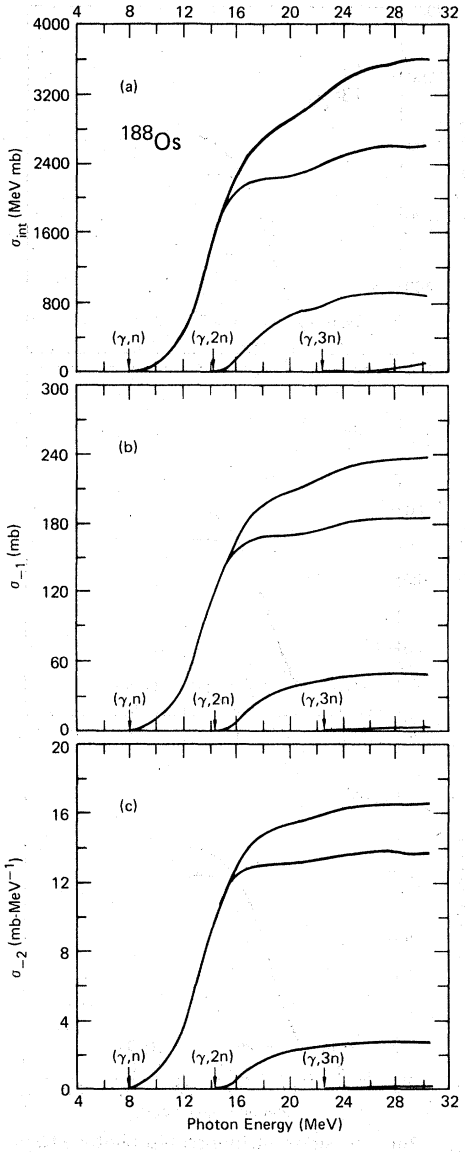

FIG. 9. Running sums of integrated cross sections for ^{188}Os: (a) σ_{int} for $\sigma(\gamma, n_t)$ (top), $\sigma(\gamma, 1n)$ (next to top), $\sigma(\gamma, 2n)$ (next to bottom), and $\sigma(\gamma, 3n)$ (bottom); (b) σ_{-1}; (c) σ_{-2}.

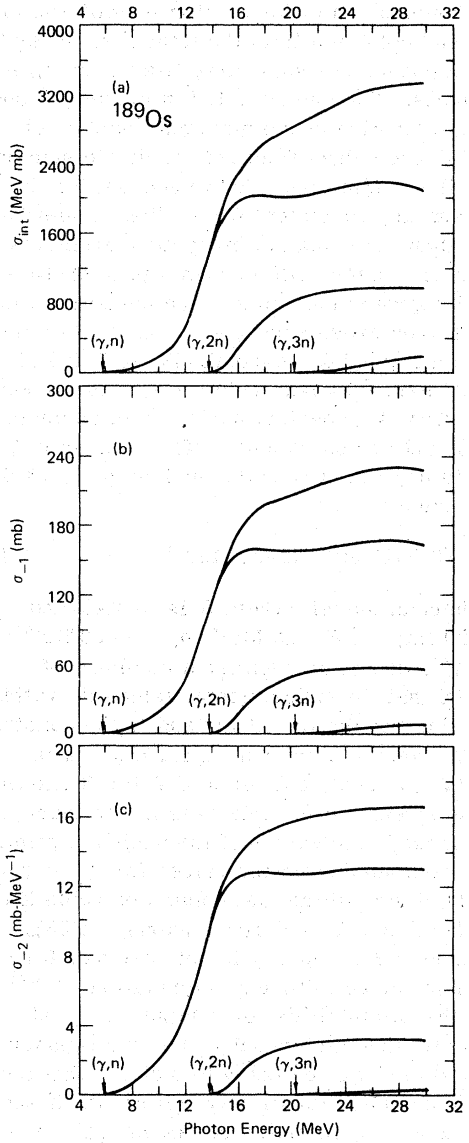

FIG. 10. Running sums of integrated cross sections for ^{189}Os: (a) σ_{int}; (b) σ_{-1}; (c) σ_{-2}.

E. Comparison with the dynamic collective model

The dynamic-collective-model treatment of the osmium isotopes by Sedlmayr *et al.*,[6] described briefly in Sec. I above, results in a definite prediction for the distribution of dipole strength in the GDR for each even-A osmium isotope, in the form of several (from 11 to 17) lines having definite energy and dipole strength (but no definite width). The authors of Ref. 6, in the absence of sufficiently detailed experimental data for the osmium isotopes, arbitrarily chose a constant width for every line of 1.5 MeV, and thereby generated predictions for GDR shapes, shown in their paper, which show dramatic structure (e.g., three distinct peaks for ^{190}Os and ^{192}Os). Unfortunately, their choice of 1.5 MeV for the widths was unrealistic, as could have been predicted from previous measurements done with monoenergetic photons,[19,25] although it certainly accomplishes their goal of illustrating the important effects that a phase transition might have on the shape of the GDR. The present data show shape changes that are much more subtle, if for no other reason than that the characteristic widths for structure in the GDR for these nuclei range from 2.5 to

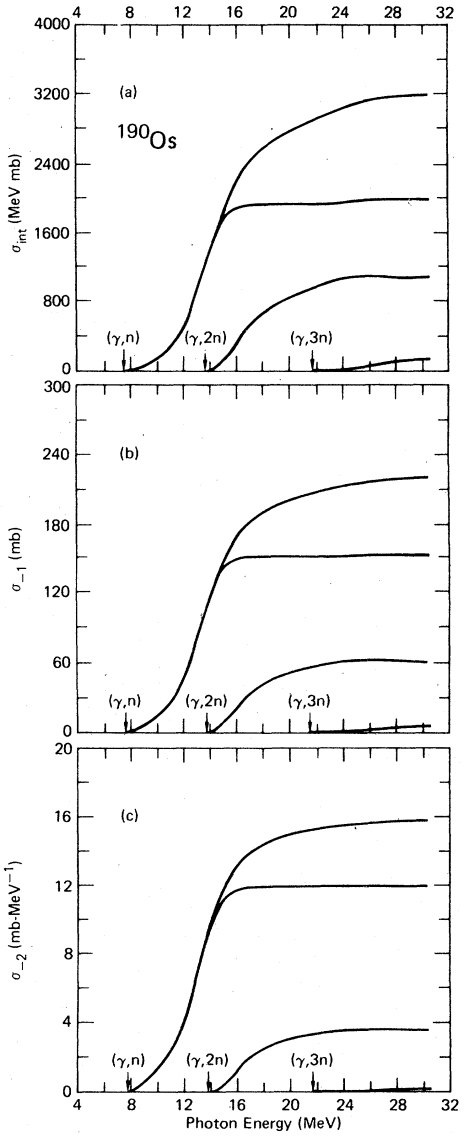

FIG. 11. Running sums of integrated cross sections for ^{190}Os: (a) σ_{int}; (b) σ_{-1}; (c) σ_{-2}.

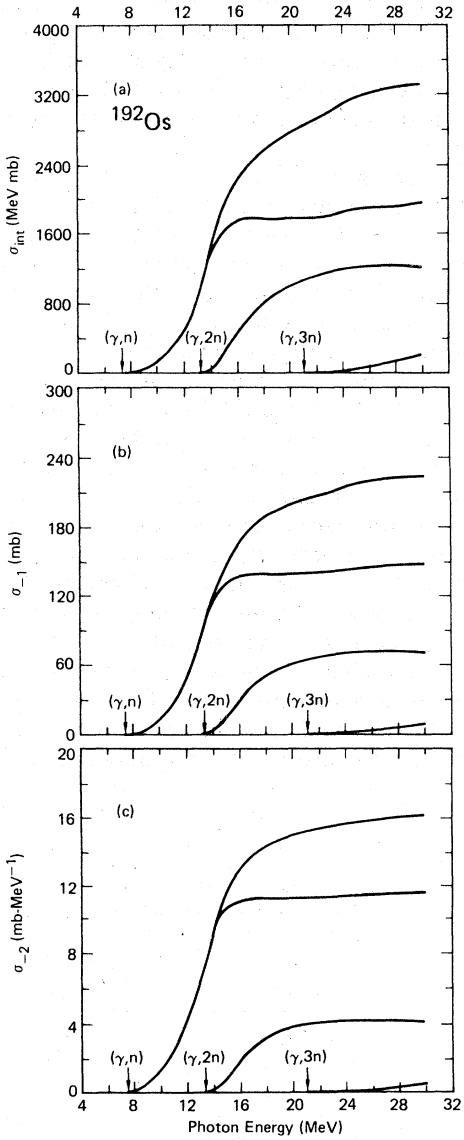

FIG. 12. Running sums of integrated cross sections for ^{192}Os: (a) σ_{int}; (b) σ_{-1}; (c) σ_{-2}.

4.4 MeV (see Table III); this tends to damp out the more dramatic effects.

In order to compare the predictions of Ref. 6 with the present results, the width of the lines was allowed to vary, along with the absolute normalization of the summed strength of all the lines for a given isotope. The data were fitted (over the energy range from 10.8 to 18.8 MeV, as before) with a constant width for every line for a given isotope. The resulting fitted curves are shown, together with the total cross-section data, in Fig. 13, and the parameters resulting from these two-parameter fits to the data are given in Table XI. It can be seen that the widths obtained from these fits lie between 2.6 and 3.0 MeV, within the expected range mentioned above, but the values for χ^2 are much larger than those for the two-component Lorentz-curve fits of Table III, and comparable (except for the case of ^{188}Os) to those for single-component Lorentz-curve fits (Sec. III C above).

It can be seen from the values of the Lorentz parameters listed in Table III that the width increases with the energy of the Lorentz lines, as is the case for all deformed nuclei studied previously.[16,19,25,37] Therefore, the attempt was made to achieve better fits to the data by allowing the widths of the lines for each isotope to vary according to an arbitrary power of the resonance energy (for the lines),[37,38] but no significant improvement in the χ^2 values for the resulting three-parameter fits was achieved.

The result of this analysis, then, is not satisfactory with respect to the details of the theoretical calculation of Sedlmayr *et al.*, especially for ^{190}Os and ^{192}Os, for which the χ^2 values show that these fits are no better than single-component Lorentz curves. Nevertheless, as is discussed in Sec. III G below, the general conclusion derived from the present experimental evidence, namely, that there is a nuclear-shape phase transition between ^{188}Os and ^{190}Os, is in agreement with the

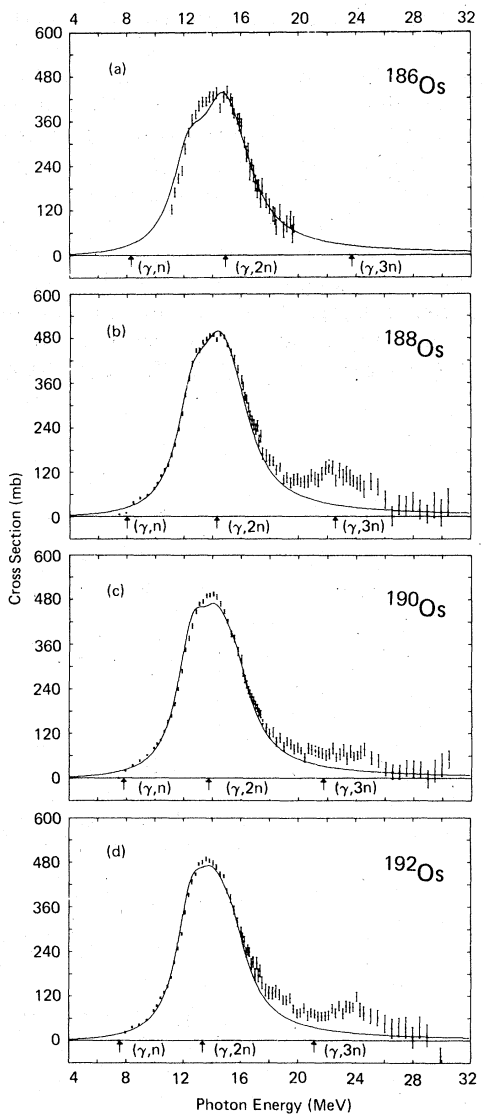

FIG. 13. Total photoneutron cross sections fitted with curves based upon the theoretical predictions of Ref. 6 (solid lines); (a) for ^{186}Os; (b) for ^{188}Os; (c) for ^{190}Os; (d) for ^{192}Os.

TABLE XI. Parameters of dynamic-collective-model (see Ref. 6) fits to the GDR. The fitting interval used is 10.8–18.8 MeV.

Nucleus	Number of lines fitted (see Ref. 6)	Width (MeV)	Normalization constant[a]	χ^2
^{186}Os	14	3.02	0.99	3.6
^{188}Os	17	2.85	0.90	5.5
^{190}Os	11	2.64	0.90	10.8
^{192}Os	12	2.64	0.87	8.8

[a] Given as a fraction of the dipole strength S_d obtained from the Lorentz parameters of Table III; $S_d = \frac{1}{2}\pi[\sigma_m(1)\Gamma(1) + \sigma_m(2)\Gamma(2)]$.

prediction of Ref. 6. This agreement in sum but not in detail points out a shortcoming in the calculation of Ref. 6; it would be interesting to see how the theoretical parameters would have to be adjusted in order to obtain a better agreement with the present data.

F. The giant quadrupole resonance

A number of theoretical calculations have been made[7-9,39-42] which attempt to describe the properties of the isovector giant quadrupole resonance (GQR) which lies higher in energy than the GDR, at least for heavy nuclei. In particular, the authors of Refs. 7, 8, and 42 predict that (a) the energy of the GQR lies at approximately $126A^{-1/3}$ MeV (with certain assumptions), or better (with fewer assumptions), that the energies of the GQR and GDR are in the ratio $3.34/2.08 = 1.60$; and (b) that the strength of the GQR is given by the hydrodynamic sum rule[7,8,39] for the second moment of the integrated quadrupole absorption cross section

$$\sigma_{-2}(\mathrm{GQR}) = \frac{\pi^2}{5}\frac{e^2}{\hbar c}\frac{NZ}{A}\frac{R^2}{Mc^2}(1+\alpha), \qquad (12)$$

where $R^2 = R_0^2 A^{2/3}$, M is the nucleon mass, and α is the amount of exhange-force enhancement of the dipole sum.

In order to delineate the structure of the GQR for the osmium isotopes, the GDR, as represented by the two-component Lorentz-curve fits to the data, was subtracted from the measured photon-absorption cross-section data points [part (a) of Figs. 2–6]; the differences, above 16 MeV, are plotted in Fig. 14. (^{186}Os is not represented in Fig. 14, since the data for that isotope do not extend high enough in energy to encompass the GQR.) The error bars shown reflect the statistical uncertainties in the data points alone, since inclusion of the additional uncertainties introduced by the subtraction of the fitted curves [which in themselves are uncertain (see Table III)] would produce only a slight effect. A glance at these GDR-subtracted data shows that only the simplest of procedures for fitting these data is justified. Accordingly, they have been fitted, between 20 and 28 MeV, with single-component Lorentz curves, shown in Fig. 14, whose characteristic parameters E_q, σ_q, and Γ_q are given in Table XII. The uncertainties in these parameters (Table XII) verify that no more complicated analysis is justified. It is unfortunate that the present data do not warrant a more sophisticated treatment, so that the evolution of the GQR, as manifested by its splitting into several substructures whose separation in energy depends upon the nuclear deformation, can be followed across this nuclear transition region; more detailed data, with much better statistics and consequently inordinately long experimental runs, would be necessary to paint such a definitive picture.

Nevertheless, the present data do give several important quantitative indications of the behavior of the GQR. The fifth column of Table XII lists the proportionality constant which results from the attempt to describe the resonance energy as being proportional to $A^{-1/3}$ (a procedure very much in vogue recently); the sixth column gives

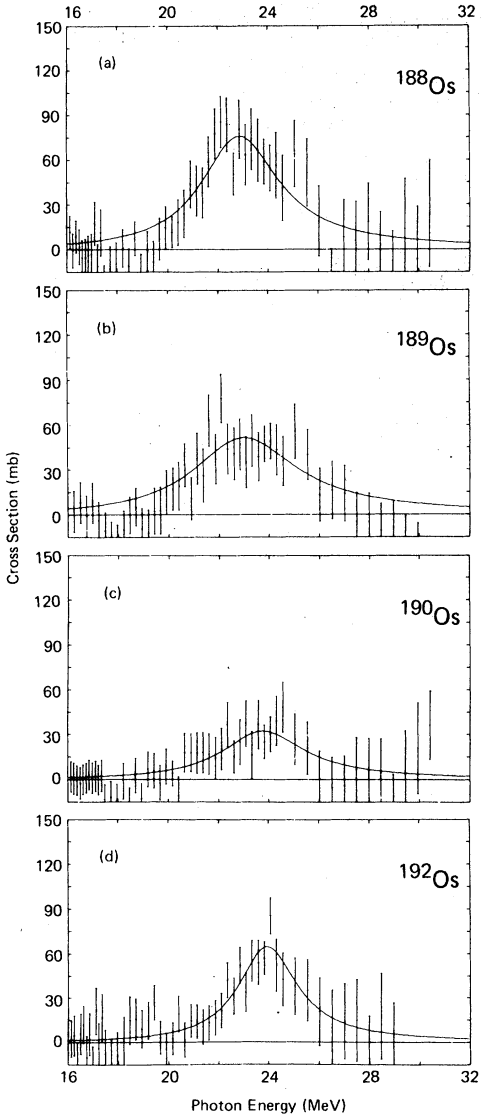

FIG. 14. Cross-section differences above the GDR; the two-component Lorentz-curve fits to $\sigma(\gamma, n_t)$ shown in part (a) of Figs. 3–6 were subtracted from the data points to give these differences, which were in turn fitted with the single-component Lorentz curves shown here as solid lines: (a) for ^{188}Os; (b) for ^{189}Os; (c) for ^{190}Os; (d) for ^{192}Os.

the resonance energy predicted[42] by the static theory mentioned above; the seventh column lists values for S_q, the strength of the GQR derived from the Lorentz fit, and the eighth column in Table XII gives that strength as a fraction of the GDR strength S_d obtained in the analogous way. Finally, the last two columns in Table XII list values for σ_{-2}(GQR) from the present experiment (computed as S_q/E_q^2) and from the sum-rule prediction of Eq. (12), taking $R_0 = 1.26$ fm as above and $(1+\alpha)$ to be S_d in sum-rule units as given in the last column of Table IX.

Two specific observations can be made from the information in Table XII. First, although the energy of the GQR (column 2 or 5) increases monotonically with A (opposite to the trend of the GDR and the theoretical prediction in column 6), neither the other Lorentz parameters nor the GQR strength S_q (columns 3, 4, and 7) exhibit any regular trend. [The GQR strength, if anything, shows a minimum at ^{190}Os (column 7, 8, and 9).] Second, once again a clear distinction can be seen between the situation for ^{188}Os and ^{189}Os on the one hand and for ^{190}Os and ^{192}Os on the other: The GQR energies for the former pair are lower and agree better with the static prediction than those for the latter pair, while the GQR strengths for the former are larger than the latter and clearly exceed the sum-rule prediction (columns 9 and 10). Over and above these, however, the general observation can be made that there no longer can be much doubt that the observed excess cross section above the GDR, as seen, for example, in Fig. 14, is almost certainly the GQR as predicted by theory and as probably seen in several previous experiments[12,19]: The overall agreement between theory and experiment (columns 2 and 6; columns 9 and 10) is just too good.

G. Nature of the phase transition

It is clear by now that there is a significant and qualitative difference between the characteristics of the photonuclear cross sections for ^{188}Os and ^{189}Os on the one hand and for ^{190}Os and ^{192}Os on the other. The evidence for this difference comes from a variety of independent features of the cross sections:

(i) the general appearance of the total cross sections and the two-component Lorentz-curve fits to them [part (a) of Figs. 3–6];

(ii) the χ^2 values for single-component Lorentz-curve fits to the total cross sections (Sec. III C and Fig. 7);

(iii) the energy of the GDR and the resulting nuclear symmetry energy (Table IV);

(iv) the distribution of strength in the GDR (R_A, Table V);

(v) the degree of nuclear deformation [η, ϵ, β_2, Q_0, and $B(E2)$, Tables V and VI];

(vi) the size of the second moment of the integrated cross section, and the resulting nuclear symmetry energy [Table X and part (c) of Figs. 9–12];

(vii) the energy of the GQR (Table XII);

(viii) the strength of the GQR (Fig. 14 and Table XII).

The sum total of this evidence strongly suggests the boundary between ^{189}Os and ^{190}Os ($N = 113$ and 114) as the location of a phase transition in the osmium isotopic series.

Kumar[43] has discussed in detail the nature of nuclear phase transitions and their relation to changes in nuclear shape. He concludes that nuclei exhibit three kinds of phase transitions: (a) spherical deformed, for which he gives as an example the well-documented evidence for the transition between ^{150}Sm and ^{152}Sm (for the GDR data, see Ref. 44); (b) superfluid normal, for which he cites the transition between the high-spin states $I = 16$ and $I = 18$ of ^{160}Dy; and (c) prolate oblate, for which he proposes the boundary between ^{190}Os and ^{192}Os. For this last case, however, the evidence presented by Kumar is far from convincing; of nine criteria listed in Ref. 43,

TABLE XII. Characteristics of the giant quadrupole resonance. The fitting interval used for the Lorentz-curve fits is 20–28 MeV.

Nucleus	E_q (MeV)	σ_q [a] (MeV)	Γ_q (MeV)	$E_q A^{1/3}$ (MeV)	$(1.60E_m)$ [b] (MeV)	$\frac{1}{2}\pi\sigma_q\Gamma_q$ (MeV mb)	(S_q/S_d) [c]	σ_{-2}(expt) [d] (mb MeV^{-1})	σ_{-2}(thy) [e] (mb MeV^{-1})
^{188}Os	22.8±0.2	76±6	3.8±0.6	131	22.7	453±107	0.12	0.87	0.49
^{189}Os	23.0±0.3	51±5	5.0±1.0	132	22.4	407±121	0.12	0.77	0.45
^{190}Os	23.8±0.3	32±4	4.0±0.9	137	22.1	202± 71	0.06	0.36	0.47
^{192}Os	23.9±0.1	65±4	2.8±0.4	138	22.1	288± 59	0.08	0.50	0.47

[a] Relative uncertainties.
[b] Theoretical prediction of Ref. 42 (see text). E_m is the GDR energy from Table IV.
[c] S_q is the quadrupole strength defined as $\frac{1}{2}\pi\sigma_q\Gamma_q$; S_d is the dipole strength defined as $\frac{1}{2}\pi[\sigma_m(1)\Gamma(1)+\sigma_m(2)\Gamma(2)]$.
[d] Computed as S_q/E_q^2.
[e] Computed from Eq. (12).

experimental evidence exists only for two. In particular, Kumar lists as one of his criteria the shift of the higher peak in the GDR from $E_>$ to $E_<$ (in the terminology of this paper, the shift of R_A from a value <1 to >1). (Of course, he was not able to cite experimental data for such a shift.)

The present experimental data thus sharply refute any proposed[5,29,30,32,43] prolate-oblate phase transition for the osmium isotopes. No osmium isotope studied here is oblate [although the data for ^{186}Os are somewhat ambiguous (see above)]. Indeed, the values for R_A are *smaller* (see Table V) for ^{190}Os or ^{192}Os than for ^{188}Os or ^{189}Os. This indicates an approach to a spherical situation with increasing mass. But this cannot be the actual case, as can be seen from the χ^2 values for one-component Lorentz-curve fits (Sec. III C above and Fig. 7). The answer might be the γ-unstable case discussed in Sec. I above, advocated most strongly by the authors of Ref. 6. Such γ-unstable nuclei would appear more spherical than prolate insofar as is indicated by the overall width of the GDR, but would not satisfy the condition of rigid sphericity implied by a single-component Lorentz-curve shape of the GDR. But if one is to conclude that this subtle but sudden observed phase transition is from a statically deformed prolate to a γ-unstable shape, then one must account for the lack of detailed agreement, noted above, between the calculations and the data.

ACKNOWLEDGMENTS

We are pleased to acknowledge valuable discussions with Professor Walter Greiner and with Dr. Frank Stephens. This work was done under the auspices of the U. S. Department of Energy under contract W-7405-ENG-48. A preliminary account of this work appeared as Bull. Am. Phys. Soc. 21, 777 (1976). The data in this paper supersede the preliminary data which appeared in Lawrence Livermore Laboratory Report No. UCRL-78482, 1976 (unpublished) as well.

[1]E. V. Inopin, Zh. Eksp. Teor. Fiz. 38, 992L (1960) [Sov. Phys.—JETP 11, 714L (1960)].
[2]K. Okamoto, Prog. Theor. Phys. 15, 75L (1956).
[3]M. Danos, Nucl. Phys. 5, 23 (1958).
[4]K. Okamoto, Phys. Rev. 110, 143 (1958).
[5]K. Kumar and M. Baranger, Nucl. Phys. A110, 529 (1968).
[6]R. Sedlmayr, M. Sedlmayr, and W. Greiner, Nucl. Phys. A232, 465 (1974); and private communication.
[7]R. Ligensa, W. Greiner, and M. Danos, Phys. Rev. Lett. 16, 364 (1966).
[8]R. Ligensa and W. Greiner, Nucl. Phys. A92, 673 (1967).
[9]T. D. Urbas and W. Greiner, Phys. Rev. Lett. 24, 1026 (1970).
[10]R. L. Bramblett, J. T. Caldwell, R. R. Harvey, and S. C. Fultz, Phys. Rev. 133, B869 (1964).
[11]R. L. Bramblett, J. T. Caldwell, G. F Auchampaugh, and S. C. Fultz, Phys. Rev. 129, 2723 (1963).
[12]S. C. Fultz, B. L. Berman, J. T. Caldwell, R. L. Bramblett, and M. A. Kelly, Phys. Rev. 186, 1255 (1969).
[13]W. Greiner, in *Proceedings of the International Conference on Photonuclear Reactions and Applications*, edited by B. L. Berman (Lawrence Livermore Laboratory, Livermore, 1973), p. 1364.
[14]Su Su, R. H. Sambell, E. G. Muirhead, and B. M. Spicer, Aust. J. Phys. 30, 677 (1977).
[15]A. M. Goryachev, G. N. Zalesnyi, S. E. Semenko, and B. A. Tulupov, Yad. Fiz. 17, 463 (1973) [Sov. J. Nucl. Phys. 17, 236 (1973)].
[16]B. L. Berman, M. A. Kelly, R. L. Bramblett, J. T. Caldwell, H. S. Davis, and S. C. Fultz, Phys. Rev. 185, 1576 (1969).
[17]A. Veyssière, H. Beil, R. Bergère, P. Carlos, A. Leprêtre, and A. de Miniac, J. Phys. (Paris) 36, L-267 (1975).
[18]M. A. Kelly, B. L. Berman, R. L. Bramblett, and S. C. Fultz, Phys. Rev. 179, 1194 (1969).
[19]B. L. Berman and S. C. Fultz, Rev. Mod. Phys. 47, 713 (1975).
[20]J. G. Woodworth, K. G. McNeill, J. W. Jury, R. A. Alvarez, B. L. Berman, D. D. Faul, and P. Meyer, Lawrence Livermore Laboratory Report No. UCRL-77471, 1978 (unpublished).
[21]J. W. Jury, B. L. Berman, D. D. Faul, P. Meyer, K. G. McNeill, and J. G. Woodworth, Phys. Rev. C (to be published).
[22]A. H. Wapstra and K. Bos, At. Data Nucl. Data Tables 19, 215 (1977).
[23]B. L. Berman, R. L. Bramblett, J. T. Caldwell, H. S. Davis, M. A. Kelly, and S. C. Fultz, Phys. Rev. 177, 1745 (1969).
[24]B. L. Berman, J. T. Caldwell, R. R. Harvey, M. A. Kelly, R. L. Bramblett, and S. C. Fultz, Phys. Rev. 162, 1098 (1967).
[25]B. L. Berman, Lawrence Livermore Laboratory Report No. UCRL-78482, 1976 (unpublished).
[26]M. V. Hoehn, E. B. Shera, Y. Yamazaki, and R. M. Steffen, Phys. Rev. Lett. 39, 1313 (1977).
[27]W. T. Milner, F. K. McGowan, R. L. Robinson, P. H. Stelson, and R. O. Sayer, Nucl. Phys. A177, 1 (1971).
[28]S. A. Lane and J. X. Saladin, Phys. Rev. C 6, 613 (1972).
[29]U. Götz, H. C. Pauli, K. Alder, and K. Junker, Phys. Lett. 38B, 274 (1972).
[30]S. Gabrakov, T. Kaniowska, and M. Zielińska-Pfabé, Acta Phys. Pol. B5, 295 (1974).
[31]C. Ekström, H. Rubinsztein, and P. Möller, Phys. Scr. 14, 199 (1976).
[32]D. Goss, Phys. Rev. C 15, 2226 (1977).
[33]A. Midgal, Zh. Eksp. Teor. Fiz. 15, 81 (1945).
[34]J. Levinger, *Nuclear Photo-Disintegration* (Oxford Univ. Press, London, 1960), p. 51.
[35]R. Bergère, H. Beil, and A. Veyssière, Nucl. Phys. A121, 463 (1968).
[36]A. Veyssière, H. Beil, R. Bergère, P. Carlos, and

A. Leprêtre, Nucl. Phys. A159, 561 (1970).
[37]R. L. Bramblett, S. C. Fultz, and B. L. Berman, *Proceedings of the International Conference on Photonuclear Reactions and Applications*, edited by B. L. Berman (Lawrence Livermore Laboratory, Livermore, 1973), p. 13.
[38]M. Danos and W. Greiner, Phys. Rev. 138, B867 (1965).
[39]Yu. K. Khoklov, Zh. Eksp. Teor. Fiz. 32, 124 (1957) [Sov. Phys.—JETP 5, 88 (1957)].
[40]V. G. Shevchenko, N. P. Yudin, and B. A. Yur'ev, Zh. Eksp. Teor. Fiz. 45, 180 (1963) [Sov. Phys.—JETP 18, 128 (1964)].
[41]A. Lushnikov and M. Urin, Yad. Fiz. 3, 436 (1965) [Sov. J. Nucl. Phys. 1, 311 (1965)].
[42]M. Danos, W. Greiner, and B. C. Kohr, Univ. of Freiburg report, 1964 (unpublished).
[43]K. Kumar, in *The Electromagnetic Interaction in Nuclear Spectroscopy*, edited by J. Hamilton (North-Holland, Amsterdam, 1975), p. 119.
[44]P. Carlos, H. Beil, R. Bergère, A. Leprêtre, A. de Miniac, and A. Veyssière, Nucl. Phys. A225, 171 (1974).